Stop-Flow Analysis of Cooperative Interactions between GLUT1 Sugar Import and Export Sites†

Lisa A. Sultzman and Anthony Carruthers*

Department of Biochemistry and Molecular Biology, University of Massachusetts Medical School, 55 Lake Avenue North, Worcester, Massachusetts 01655

Received January 20, 1999; Revised Manuscript Received March 19, 1999

ABSTRACT: The human erythrocyte sugar transporter is thought to function either as a simple carrier (sugar import and sugar export sites are presented sequentially) or as a fixed-site carrier (sugar import and sugar export sites are presented simultaneously). The present study examines each hypothesis by analysis of the rapid kinetics of reversible cytochalasin B binding to the sugar export site in the presence and absence of sugars that bind to the sugar import site. Cytochalasin B binding to the purified, human erythrocyte glucose transport protein (GLUT1) induces quenching of GLUT1 intrinsic tryptophan fluorescence. The time-course of GLUT1 fluorescence quenching reflects a second-order process characterized by simple exponential kinetics. The pseudo-first-order rate constant describing fluorescence decay (k_{obs}) increases linearly with [cytochalasin B] while the extent of fluorescence quenching increases in a saturable manner with [cytochalasin B]. Rate constants for cytochalasin B binding to GLUT1 (k_1) and dissociation from the GLUT1·cytochalasin B complex (k_{-1}) are obtained from the relationship: $k_{obs} = k_{-1} + k_1$[cytochalasin B]. Low concentrations of maltose, D-glucose, 3-*O*-methylglucose, and other GLUT1 import-site reactive sugars increase $k_{-1(app)}$ and reduce $k_{1(app)}$ for cytochalasin B interaction with GLUT1. Higher sugar concentrations decrease $k_{1(app)}$ further. The simple carrier mechanism predicts that $k_{1(app)}$ alone is modulated by import- and export-site reactive sugars and is thus incompatible with these findings. These results are consistent with a fixed-site carrier mechanism in which GLUT1 simultaneously presents cooperative sugar import and export sites.

Various models have been suggested for protein-mediated, passive sugar transport *(1)*, but only two are supported by significant bodies of experimental data. The simple carrier hypothesis proposes that the glucose transporter sugar import and sugar export pathways are presented sequentially to available substrate *(2, 3)*. The fixed-site carrier proposes that the transporter presents sugar import and sugar export pathways simultaneously *(1, 4, 5)*.

Krupka and Devés *(6)* recognized that simple measurements of the concentration dependence of the initial rates of sugar transport can be insufficient to distinguish these carrier mechanisms. Their analysis led to the important suggestion of measuring zero-trans sugar fluxes (sugar uptake or exit in the absence of transported sugar at the opposite side of the membrane) in the presence of two reversible, transport inhibitors. One inhibitor must compete with transported sugar for binding to the sugar import site while the second inhibitor must compete with transported sugar at the export site. Because import and export sites of the fixed-site carrier are presented simultaneously for occupancy by substrate, the presence of extracellular inhibitor should be without effect on intracellular inhibitor binding to the export site. Conversely, if the carrier were a simple carrier, the presence of extracellular inhibitor would trap the carrier in the import conformation, reducing the amount of carrier available for reaction with intracellular inhibitor. In this way, extracellular inhibitor will act as a competitive inhibitor of intracellular inhibitor binding and vice versa.

The results of their studies (using cytochalasin B and phloretin as export- and import-site reactive inhibitors, respectively) suggested that the human erythrocyte sugar transporter was either a simple carrier or a modified fixed-site carrier *(6)*. The modified fixed-site carrier is a fixed-site carrier that allows for strong negative cooperativity between import and export sites. Thus, inhibitor occupancy of one site causes markedly reduced affinity of the opposite site for inhibitor. Subsequent steady-state transport and equilibrium ligand binding studies from this laboratory *(7−9)* have supported the modified fixed-site carrier hypothesis.

The central assumption of these earlier studies requires that competitive inhibitors of sugar transport interact with sugar import or export sites. This assumption has not been tested directly. It is not necessary for a ligand pair to interact at the same site in order to show competitive binding *(10)*. Binding sites can be distinct but mutually exclusive because: (1) bound inhibitor and substrate share overlapping space beyond the carrier−ligand contact sites (extrinsic steric overlap); (2) binding of inhibitor at one site promotes a conformational change at a second site which prevents its occupancy by substrate and vice versa (negative cooperativity).

† This work was supported by NIH Grant DK 44888.

* To whom correspondence should be addressed. E-mail: anthony.carruthers@umassmed.edu. Telephone: 508 856 5570. FAX: 508 856 6231.

10.1021/bi990130o CCC: $18.00
Published on Web 05/01/1999

These considerations prompted us to evaluate the possibility that the sugar transport inhibitors cytochalasin B (a competitive inhibitor of sugar export) and phloretin or extracellular maltose (competitive inhibitors of sugar import) do not bind directly at transport sites. Instead, these inhibitors bind within and block pathways that direct substrate to the transport site. If cis-inhibitor and substrate binding sites are mutually exclusive through extrinsic steric overlap or negative cooperativity, this allows for competition between substrate and inhibitor for binding at the same side of the membrane. Binding of cis- and trans-inhibitors at opposite ends of the transport pathway need not be exclusive and can even show cooperativity. If the transport mechanism located within such a transport pathway were a simple carrier, transport would appear to be mediated by a simple carrier mechanism, but its inhibition by cis- and trans-inhibitors would suggest a fixed-site mechanism.

In the present study we examine the transient kinetics of CCB[1] binding to the purified glucose transport protein (GLUT1) to ask the following: Does GLUT1 present maltose and CCB binding sites simultaneously? We demonstrate that CCB and high-affinity maltose binding sites coexist in GLUT1. We then ask whether maltose and CCB binding sites are intrinsic or extrinsic to the GLUT1 catalytic center. Our findings support the hypothesis that maltose and CCB binding sites correspond to substrate binding sites. We therefore conclude that the glucose transporter functions as a fixed-site carrier.

MATERIALS AND METHODS

Materials. Human blood was obtained from the American Red Cross. Outdated human blood was obtained from the University of Massachusetts Blood Bank. Radiochemicals were purchased from New England Nuclear (Boston, MA). Octyl-β-glucoside was purchased from Calbiochem (La Jolla, CA). All other reagents were purchased from Sigma Chemicals (St. Louis, MO).

Solutions. Saline consisted of 150 mM NaCl, 10 mM TrisHCl, 0.5 mM EDTA, pH 7.4. Tris medium consisted of 50 mM TrisHCl, 0.2 mM EDTA, pH 7.4. Lysis medium contained 10 mM TrisHCl, 0.2 mM EDTA, pH 7.2.

Human Erythrocytes and Purified GLUT1. Human red cells (RBCs) were harvested from whole blood by centrifugation at 30000*g* for 15 min at 4 °C. Serum, white cells, and platelets were aspirated, and the erythrocyte pellet was resuspended in 10 volumes of saline. This red cell suspension was subjected to two additional centrifugation/wash cycles. The final red cell pellet was resuspended in 40 volumes of saline and incubated at 20 °C for 20 min to deplete intracellular D-glucose levels. D-Glucose-depleted erythrocytes were collected by centrifugation and stored in saline on ice.

Tetrameric GLUT1 was purified from washed, human erythrocytes as described previously *(11)*. Erythrocyte membranes containing only integral membrane proteins were prepared by alkaline extraction of hypotonically lysed erythrocytes as described in *(12)*.

[1] Abbreviations: GLUT1, human erythrocyte glucose transport protein; 3OMG, 3-*O*-methylglucose; CCB, cytochalasin B; EDTA, ethylenediaminetetraacetic acid; NATA, *N*-acetyltryptophanamide; NBS, *N*-bromosuccinamide; Tris-HCl, tris(hydroxymethyl)aminomethane.

Sugar Transport in RBCs. 3-*O*-Methylglucose uptake by D-glucose-free red cells at 100 μM sugar and 4 °C was measured at 0 and 30 s and expressed relative to the equilibrium 3-*O*-methylglucose space of the cell as described previously *(9)*.

[^{3}H]Cytochalasin B Binding to Isolated GLUT1 and to Red Cell Membrane-Resident GLUT1. Cytochalasin B binding at 4 °C was measured as described previously *(9)*. Briefly, membranes containing GLUT1 (20−50 μg of protein) were resuspended in 2−3 volumes of Tris medium containing [^{3}H]-CCB, unlabeled CCB (0−2000 nM), and cytochalasin D (CCD, 10 μM). CCD competitively inhibits CCB binding to non-GLUT1 red cell proteins *(13)*. Aliquots of total [^{3}H]-CCB were sampled, the membranes containing GLUT1 sedimented by centrifugation (14000*g* for 10 min), and samples of free [^{3}H]-CCB obtained from the supernatant. Bound [^{3}H]-CCB is computed as the difference between total and free [^{3}H]-CCB.

Steady-State, GLUT1 Intrinsic Fluorescence. GLUT1 intrinsic tryptophan fluorescence at 20 °C was monitored using a Spex Fluoromax 2 fluorometer. Excitation was at 284 nm, and emission was monitored at wavelengths between 250 and 750 nm. Slit widths of 5 nm were used for both excitation and emission. The light path was 1 cm. Unsealed GLUT1 proteoliposomes (50 μg of protein/mL of Tris medium) were titrated against ligand (CCB in Tris medium containing unsealed GLUT1 proteoliposomes at 50 μg·mL^{-1}), and steady-state fluorescence was measured following each addition of ligand. Maximum GLUT1 emission was observed at 333 nm. The reduced fluorescence promoted by ligand binding was not associated with a red or blue shift of the emission spectrum.

Stopped-Flow Fluorescence Measurements. The time-course of ligand binding induced GLUT1 fluorescence quenching was monitored using a Hi-Tech Scientific SF-61DX2 stopped-flow system. GLUT1 (50 μL of a sample containing 20 μg of GLUT1/mL of saline) was mixed with CCB (50 μL of saline containing 0−8 μM CCB) and driven into the light path of the flow cell within 1 ms by using a pneumatic drive system. Excitation was at 280 nm, and emission at all wavelengths above 320 nm was collected by use of a photomultiplier. Excitation slit widths of 5 nm were used. A reference photomultiplier was used to monitor fluctuations in the output of the source of excitation and thereby reduce background noise. The flow cell and solution reservoirs were maintained at 20 °C using a temperature-controlled circulating water bath. Data were sampled every 10 μs and, in most experiments, averaged over a time interval of 1 ms.

The dead time of the mixing path (1 ms) was confirmed by analysis of the time course of *N*-acetyltryptophanamide (NATA) fluorescence quenching by *N*-bromosuccinamide (NBS) at 20 °C. NATA (41 μM) and NBS (1020 μM) were prepared in buffer containing 50 mM Na_2HPO_4, 50 mM NaH_2PO_4·H_2O, pH 6.9. Equal volumes of NATA and NBS were driven into the light path. Fluorescence was normalized to E_0(100%) − fluorescence obtained when NATA- and NBS-free buffer are mixed. The fluorescence E_1 (measured at the start of data capture when solution driven by the pneumatic drives forces the piston of the stopping syringe to hit the stopping block and to trigger data collection) is related to E_0 and the dead time (t_d) of the instrument in the

following manner:

$$t_d = k \ln \frac{E_0}{E_1}$$

where k is the first-order rate constant describing the rate of NATA quenching by NBS. The time-course of NATA quenching is consistent with a first-order process and is characterized by $k = 336 \pm 3\ s^{-1}$ ($n = 11$) under the conditions described above. This compares with an expected value of 366 s^{-1} as extrapolated from *(14)*. E_0/E_1 averaged 1.67 ± 0.02, indicating a dead time of 1.53 ± 0.03 ms.

In experiments where sugar modulation of CCB binding was measured, GLUT1- and CCB-containing solutions also contained equal concentrations of the sugar of interest (e.g., D-glucose) prior to mixing and injection into the light path. Since sugar concentrations were varied over the range 0−100 mM, saline also contained 100 mM L-glucose or sucrose to control for changes in osmolality. L-Glucose and sucrose do not interact with GLUT1 *(15)*. Saline containing 100 mM active sugar (e.g., D-glucose or maltose) was mixed with saline containing 100 mM L-glucose or sucrose to produce appropriate concentrations of active sugar. GLUT1 intrinsic fluorescence as measured in the Hi-Tech Scientific SF-61DX2 stopped-flow system is not affected significantly by the sugars employed in this study.

Curve-Fitting Procedures. Time-course data acquired using the Hi-Tech Scientific SF-61DX2 stopped-flow system were analyzed using the software package KinetAsyst 2 (Hi-Tech Scientific, Salisbury, U.K.). Fluorescence decay records were analyzed by nonlinear regression assuming that decay was described by single or multiple exponential components. Time-course data were also exported to text files for subsequent analysis by nonlinear regression using the software package KaleidaGraph 3.08d (Synergy Software, Reading, PA).

In experiments where sugar modulation of k_{obs} for CCB binding to GLUT1 is presented graphically in the form k_{obs} versus [sugar], data were analyzed by nonlinear regression according to the fixed-site model for ligand binding (see Discussion for rationale). The equation takes the form (see Discussion):

$$k_{obs} = \frac{k_{-1} + k_{-1}'\dfrac{M2}{\alpha K_{M2}}}{1 + \dfrac{M2}{\alpha K_{M2}}} + [CCB]\frac{k_1 + k_1'\dfrac{M2}{\alpha K_{M2}}}{1 + \dfrac{M1}{K_{M1}} + \dfrac{M2}{K_{M2}} + \dfrac{M1M2}{\beta K_{M1} K_{M2}}}$$

where

$$\alpha = \frac{k_{-1}'}{k_1'}\frac{k_1}{k_{-1}}$$

The curves drawn through the points were computed using these expressions, and the resulting parameters are summarized in the figure legends.

Analytical Procedures. Protein assays and SDS-slab (18%) polyacrylamide gel electrophoresis of membrane proteins were carried out as described previously *(11)*.

RESULTS

GLUT1 Proteoliposomes. Isolated, nonreduced, detergent-solubilized GLUT1 copurifies with solubilized erythrocyte lipid *(16)*. In the absence of exogenous phospholipid, detergent removal produces small proteoliposomes of 0.25 μm diameter or less as judged by phase contrast microscopy. Two lines of evidence indicate that GLUT1 proteoliposomes are highly permeable to macromolecules present in bulk solution. (1) Proteoliposomal GLUT1 is simultaneously accessible to antibodies that bind specifically to endo- or to exofacial GLUT1 epitopes *(17)*. (2) Trypsin exposure produces quantitative removal of the GLUT1 carboxyl terminus as judged by immunoblot analysis using anti-GLUT1 carboxyl-terminal peptide antibodies *(18)*.

Steady-State Ligand Binding to GLUT1 Proteoliposomes. CCB is an export-site-reactive, GLUT1 ligand *(4, 8)*. $K_{d(app)}$ for equilibrium CCB binding to purified GLUT1 was obtained by measuring ligand-induced quenching of GLUT1 intrinsic tryptophan fluorescence and by measuring [^{3}H]-CCB binding to GLUT1 in the presence or absence of competing unlabeled substrate. GLUT1 CCB binding capacity was obtained from [^{3}H]-CCB binding studies. [^{3}H]-CCB binding to isolated, nonreduced GLUT1 is characterized by $K_{d(app)} = 184 \pm 36$ nM CCB and by $B_{max} = 0.50 \pm 0.14$ mol of CCB/mol of GLUT1 (9.1 pmol of CCB/μg of GLUT1 protein; $n = 8$). These results are consistent with previous measurements from this laboratory *(17)*.

Rapid Kinetics of Ligand Binding to GLUT1 Proteoliposomes. GLUT1 intrinsic fluorescence falls by approximately 5−10% when purified, nonreduced, human GLUT1 (10 μg/mL) is mixed with 4 μM CCB (Figure 1). Analysis of the steady-state fluorescence of the GLUT1·CCB complex versus unliganded GLUT1 indicates that CCB binding quenches fluorescence uniformly at all wavelengths (320−500 nm). Thus, altered fluorescence above 320 nm does not result from a ligand-induced shift in the emission spectrum of nonreduced GLUT1.

The time-course of CCB-promoted fluorescence decay was observed over intervals of 1−10 s and is consistent with a single exponential decay process. Analyses that assume two or three time-resolved exponential quenching components do not significantly improve correspondence between data and predicted results. CCB-promoted fluorescence quenching is characterized by a first-order rate constant k_{obs} and by an extent of fluorescence change (ΔF; see Figure 1). k_{obs} may directly reflect CCB binding to GLUT1 (a second-order process). If the binding reaction is too rapid to resolve, k_{obs} may represent the time constant of a putative, conformational change (a first-order reaction) promoted by CCB binding to GLUT1.

To distinguish these possibilities, k_{obs} was determined over a range of CCB concentrations. Figure 2A shows that k_{obs} increases linearly with [CCB]. This result is expected for a second-order reaction and takes the form (see ref *19*):

$$[GLUT1] = [GLUT1]_e + ([GLUT1]_0 - [GLUT1]_e)e^{-(k_1 CCB + k_{-1})t}$$

where [GLUT1], $[GLUT1]_e$, and $[GLUT1]_0$ are the concentrations of unliganded GLUT1 present at times t, at equilibrium, and at time zero, respectively, and k_1 and k_{-1} are

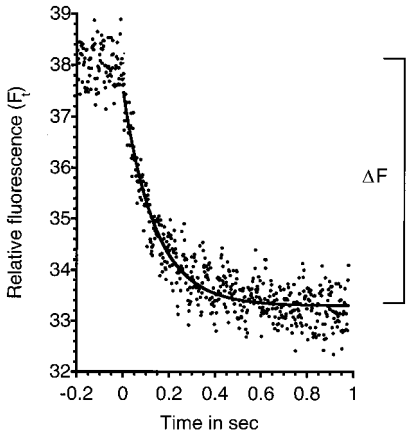

FIGURE 1: Time course of CCB-induced, GLUT1 intrinsic tryptophan fluorescence quenching. On the ordinate is the relative GLUT1 fluorescence (F_t) in arbitrary units. On the abscissa is time in seconds. Excitation was at 280 nm. Emission was collected at all wavelengths above 320 nm. Data were sampled at 10 kHz and averaged over 2 ms intervals. At zero time, 50 μL of GLUT1 (20 μg/mL of saline) was mixed with 50 μL of saline containing 8 μM CCB. Mixing is complete within 1.5 ms (see Materials and Methods), and fluorescence decays until a new steady-state (F_e) is achieved at approximately 1 s. Mixing GLUT1 and CCB-free saline produces a stable fluorescence record which does not decay over intervals of 10 s or greater (data not shown). This is the record shown prior to zero time. The curve drawn through the data points was computed by nonlinear regression assuming a single exponential decay process described by

$$F_t = F_e + \Delta F_e^{-k_{obs}t}$$

where F_e is that fluorescence observed when the reaction between GLUT1 and CCB achieves equilibrium, ΔF is the difference between GLUT1 fluorescence at zero time and equilibrium, and k_{obs} is a first-order rate constant. For this data set, $F_e = 33.29 \pm 0.03$, $\Delta F = 4.2 \pm 0.1$, and $k_{obs} = 7.2 \pm 0.3$ s^{-1} ($R^2 = 0.87$).

second- and first-order rate constants describing CCB association with and dissociation from GLUT1, respectively. The rate constant k_{obs} is thus

$$k_{obs} = k_1[CCB] + k_{-1}$$

k_1 and k_{-1} are obtained as the slope and y-intercepts, respectively, of a plot of k_{obs} versus [CCB] (Figure 2A). The computed values are $k_1 = 2.8 \times 10^6$ M^{-1}·s^{-1} and $k_{-1} = 0.7$ s^{-1}. The ratio k_{-1}/k_1 (0.25 μM CCB) is $K_{d(app)}$ for CCB binding to GLUT1.

The change in equilibrium fluorescence ($-\Delta F$) produced upon CCB binding is related to [CCB] by a simple Michaelis−Menten function with a $K_{d(app)}$ of 0.24 μM CCB and a maximum fluorescence quenching ($-\Delta F_m$) of 4.5% (Figure 2B). The close correspondence between $K_{d(app)}$ obtained by analysis of the rate (k_{obs}) of fluorescence quenching and $K_{d(app)}$ obtained from the extent ($-\Delta F$) of fluorescence quenching supports the conclusion that the rate-limiting step in CCB-induced GLUT1 fluorescence quenching is CCB association with GLUT1.

Effects of GLUT1 Ligands on CCB Binding. The simple carrier hypothesis requires that the glucose carrier cycles between two states in the absence of sugar. The *e2* state presents a sugar import site, and the *e1* state presents a sugar export site. CCB is an *e1*-reactive ligand only. Addition of an *e2*-reactive but nontransportable ligand such as extracellular maltose will trap the carrier in an *e2* state (*e2*·maltose),

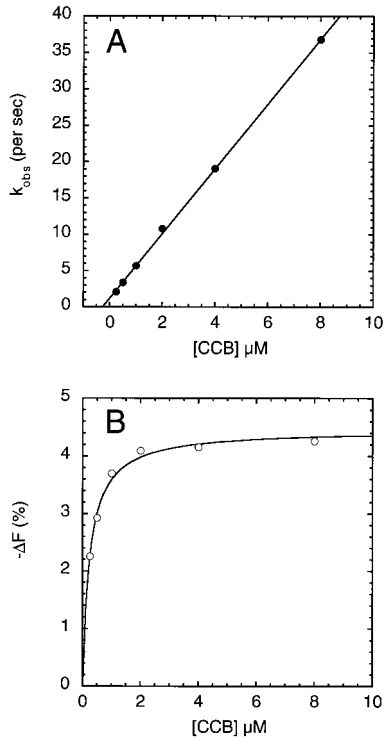

FIGURE 2: Effect of [CCB] on k_{obs} and ΔF for GLUT1 fluorescence decay. The experiment of Figure 1 was repeated 4 or more times at several CCB concentrations. Time course data were averaged for each CCB concentration and analyzed as in Figure 1 to obtain k_{obs} and ΔF. (A) Dependence of k_{obs} on [CCB]. On the ordinate is k_{obs} in s^{-1}. On the abscissa is [CCB] in μM. The line drawn through the points was computed by linear regression and takes the form

$$k_{obs} = k_{-1} + k_1[CCB]$$

where k_{-1} (y-intercept) is a first-order rate constant describing CCB dissociation from the GLUT1·CCB complex and k_1 (slope) is a second-order rate constant describing CCB and GLUT1 association to form the GLUT1·CCB complex. According to this analysis, $k_1 = 4.45 \pm 0.05$ μM^{-1} s^{-1} and $k_{-1} = 1.27 \pm 0.19$ s^{-1} ($R^2 = 0.999$). (B) Dependence of ΔF on [CCB]. On the ordinate is ΔF in arbitrary units. On the abscissa is [CCB] in μM. The curve drawn through the points was computed by nonlinear regression and takes the form

$$\Delta F = \Delta F_{max}[CCB]/(K_{d(app)} + [CCB])$$

where ΔF_{max} is the maximum ΔF produced at saturating [CCB] and $K_{d(app)}$ is that [CCB] producing $\Delta F = 0.5\Delta F_{max}$. According to this analysis, $\Delta F_{max} = 4.5 \pm 0.1$ and $K_{d(app)} = 0.24 \pm 0.02$ μM CCB ($R^2 = 0.99$).

reducing the amount of *e1*-state carrier available for reaction with CCB. Addition of an *e1* ligand such as intracellular maltose also reduces the amount of free *e1*-state carrier available for reaction with CCB by direct competition. In both instances, k_{obs} for CCB binding is decreased because the rate of CCB binding is proportional to $k_1[e1][CCB]$. Thus, the simple carrier model predicts that CCB binding and maltose (intra- and extracellular) binding show simple competitive inhibition.

The fixed-site carrier predicts a rather different result. Because external (*e2*) and internal (*e1*) ligand binding sites coexist, an *e2*-reactive ligand will not affect the availability of the *e1* site and therefore fails to affect CCB binding at *e1*. However, a competing *e1*-reactive ligand such as intracellular maltose would reduce the amount of fixed-site carrier *e1* site available for reaction with CCB by direct competition for binding. If the fixed-site carrier ligand

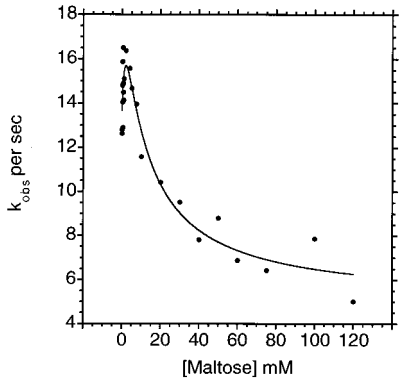

FIGURE 3: Effect of [maltose] on k_{obs} for CCB (4 μM)-promoted GLUT1 fluorescence decay. GLUT1 and CCB solutions contained identical [maltose] (0−240 mM) prior to rapid mixing. The experiment of Figure 1 was repeated at least 4 times at each maltose concentration. Time course data were averaged for each [maltose] employed and analyzed as in Figure 1 to obtain k_{obs} for fluorescence decay. On the ordinate is k_{obs} in s^{-1}. On the abscissa is [maltose] in mM. The curve drawn through the points was computed by nonlinear regression assuming that CCB and maltose binding to GLUT1 is consistent with a fixed-site carrier mechanism (see Materials and Methods). According to this analysis, $k_{-1} = 1.53$ s^{-1}, $k_{-1}' = 4.99$ s^{-1}, $K_{M2} = 1.72$ mM, $K_{M1} = 22.6$ mM, $k_1 = 3.03$ $\mu M^{-1}\cdot s^{-1}$, $k_1' = 6.39$ $\mu M^{-1}\cdot s^{-1}$, and $\beta = 0.47$ ($R^2 = 0.92$). This experiment was repeated 5 times with similar results (see Table 1).

binding sites (*e1* and *e2*) interact cooperatively, an *e2*-reactive ligand could affect CCB binding at *e1* and vice versa. Thus, occupation of a fixed-site carrier *e2* site by extracellular maltose could increase (positive cooperativity) or reduce (negative cooperativity) the affinity of the *e1* site for CCB.

Figure 3 shows the effects of increasing concentrations of maltose on k_{obs} for CCB binding to purified GLUT1. k_{obs} increases at low maltose concentrations and then decreases in a saturable manner at high [maltose]. This observation is not a purification artifact because a similar result is also obtained using erythrocyte membranes containing integral membrane proteins but lacking peripheral proteins (Figure 4A).

Analysis of the [CCB] dependence of k_{obs} at varying [maltose] allows direct determination of the mode of action of maltose on k_1 and k_{-1}. Figure 4B shows that maltose increases $k_{-1(app)}$ but reduces $k_{1(app)}$ for CCB interaction with membrane-resident GLUT1. Similar experiments with purified GLUT1 (Figure 5A) show that low [maltose] reduces $k_{1(app)}$ but increases $k_{-1(app)}$. At higher maltose concentrations, $k_{1(app)}$ is further reduced. Increased $k_{-1(app)}$ is not predicted by the simple carrier hypothesis and suggests that CCB and extracellular maltose can bind to GLUT1 simultaneously but that CCB dissociates more rapidly from the maltose·GLUT1·CCB complex than it does from the GLUT1·CCB complex. $K_{d(app)}$ for CCB binding increases rapidly and in a saturable manner at low [maltose] but increases linearly at higher [maltose] (Figure 5B). This result is similar to that observed for ethylidene glucose modulation of $K_{d(app)}$ for equilibrium CCB binding to erythrocyte membranes (*7*) and is also observed for maltose modulation of CCB binding to erythrocyte membranes depleted of peripheral membrane proteins (Figure 4B). This finding is consistent with the hypothesis that CCB and maltose compete directly for binding at the *e1* (exit) site (a low-affinity maltose site) but indirectly (with negative cooperativity) when maltose occupies the *e2* (import, high-affinity maltose site) and CCB occupies *e1*. This result is incompatible with the simple carrier hypothesis for glucose transport.

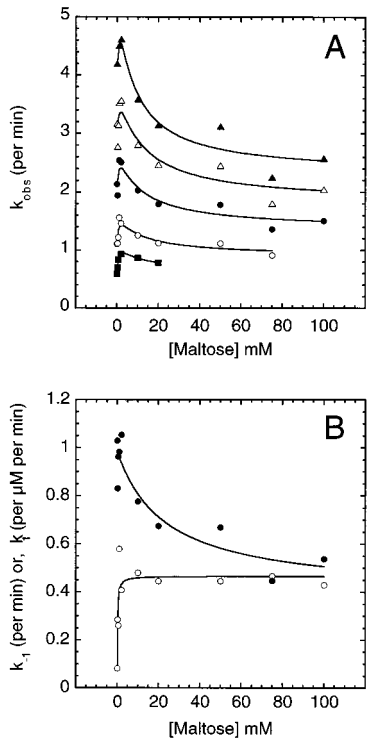

FIGURE 4: Effect of [maltose] on CCB-dependent erythrocyte integral membrane protein fluorescence quenching. Erythrocyte integral membrane proteins (100 μg of protein/mL of saline) and CCB solutions (1−8 μM) contained identical [maltose] (0−200 mM) prior to rapid mixing. Membranes and CCB solutions were mixed, and k_{obs} for fluorescence decay was calculated for each [CCB] and [maltose] as in Figures 1 and 3. (A) On the ordinate is k_{obs} in s^{-1}. On the abscissa is [maltose] in mM. Data are shown for $[CCB]_{final} = 0.5$ μM (■), 1 μM (○), 2 μM (●), 3 μM (△), and 4 μM (▲). Each point represents k_{obs} computed for four or more averaged runs. The curves drawn through the points were computed as in Figure 3 and have the following constants: 0.5 μM CCB, $k_{-1} = 0.08$ s^{-1}, $k_{-1}' = 0.64$ s^{-1}, $K_{M2} = 0.52$ mM, $K_{M1} = 165$ mM, $k_1 = 1.02$ $\mu M^{-1}\cdot s^{-1}$, $k_1' = 3.28$ $\mu M^{-1}\cdot s^{-1}$, and $\beta = 0.04$ ($R^2 = 0.97$); 1 μM CCB, $k_{-1} = 0.08$ s^{-1}, $k_{-1}' = 0.90$ s^{-1}, $K_{M2} = 0.14$ mM, $K_{M1} = 27.8$ mM, $k_1 = 1.02$ $\mu M^{-1}\cdot s^{-1}$, $k_1' = 3.04$ $\mu M^{-1}\cdot s^{-1}$, and $\beta = 0.37$ ($R^2 = 0.80$); 2 μM CCB, $k_{-1} = 0.08$ s^{-1}, $k_{-1}' = 1.36$ s^{-1}, $K_{M2} = 0.10$ mM, $K_{M1} = 32.69$ mM, $k_1 = 1.02$ $\mu M^{-1}\cdot s^{-1}$, $k_1' = 3.53$ $\mu M^{-1}\cdot s^{-1}$, and $\beta = 0.33$ ($R^2 = 0.89$); 3 μM CCB, $k_{-1} = 0.08$ s^{-1}, $k_{-1}' = 1.82$ s^{-1}, $K_{M2} = 0.07$ mM, $K_{M1} = 31.92$ mM, $k_1 = 1.02$ $\mu M^{-1}\cdot s^{-1}$, $k_1' = 4.00$ $\mu M^{-1}\cdot s^{-1}$, and $\beta = 0.36$ ($R^2 = 0.90$); 4 μM CCB, $k_{-1} = 0.08$ s^{-1}, $k_{-1}' = 2.31$ s^{-1}, $K_{M2} = 0.11$ mM, $K_{M1} = 26.98$ mM, $k_1 = 1.02$ $\mu M^{-1}\cdot s^{-1}$, $k_1' = 4.99$ $\mu M^{-1}\cdot s^{-1}$, and $\beta = 0.28$ ($R^2 = 0.95$). (B) Effect of [maltose] on $k_{1(app)}$ and $k_{-1(app)}$ for CCB binding to GLUT1 in erythrocyte membranes depleted of peripheral membrane proteins. Data of Figure 4A were recast in the form of [CCB] (abscissa) versus k_{obs} (ordinate) for each maltose concentration employed. Linear regression analysis was performed as in Figure 2A to obtain k_{-1} (*y*-intercept) and k_1 (slope) for CCB binding at each [maltose]. These results are then plotted as k_{-1} (○, in s^{-1}) or k_1 (●, $\mu M^{-1}\cdot s^{-1}$) on the ordinate versus [maltose] (in mM) on the abscissa. The curves drawn through the points were computed assuming simple saturation kinetics and take the form

$$k = k_o + [\Delta k[\text{maltose}]/(K_{d(\text{maltose})} + [\text{maltose}])]$$

where k_0 is k_1 or k_{-1} in the absence of maltose, Δk is the increment in k_1 or k_{-1} produced upon addition of saturating [maltose], and $K_{d(maltose)}$ is that [maltose] producing half Δk. The results are: for k_{-1}, $k = 0.08$ s^{-1}, $\Delta k = 0.39$ s^{-1}, and $K_{d(maltose)} = 0.19$ mM; for k_1, $k = 1.02$ $\mu M^{-1}\cdot s^{-1}$, $\Delta k = -0.59$ $\mu M^{-1}\cdot s^{-1}$, and $K_{d(maltose)} = 23.5$ mM.

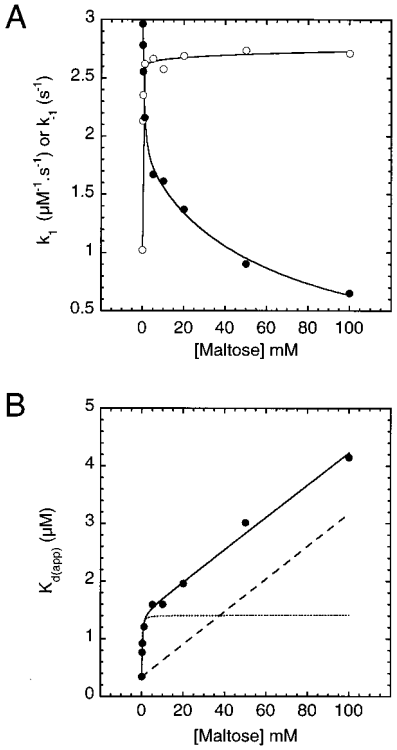

FIGURE 5: Effect of [maltose] on k_1, k_{-1}, and $K_{d(app)}$ for CCB binding to purified GLUT1. Purified GLUT1 was titrated against varying [CCB] (see Figure 2) at varying [maltose] (e.g., see Figure 4). Linear regression analysis was performed as in Figure 2A to obtain k_{-1} (*y*-intercept) and k_1 (slope) for CCB binding at each [maltose]. (A) These results are plotted as k_{-1} (○, in s^{-1}) or k_1 (●, $\mu M^{-1}\cdot s^{-1}$) on the ordinate versus [maltose] (in mM) on the abscissa. The curves drawn through the points were computed allowing for two saturable components of maltose modulation of CCB binding and take the form

$$k = k_o + [\Delta k_1[\text{maltose}]/({}^1K_{d(\text{maltose})} + [\text{maltose}]) + \Delta k_2[\text{maltose}]/({}^2K_{d(\text{maltose})} + [\text{maltose}])]$$

where k_o is k_1 or k_{-1} in the absence of maltose, Δk_1 and Δk_2 are the increments in k_1 or k_{-1} produced by saturable components 1 and 2 upon addition of saturating [maltose], and ${}^1K_{d(\text{maltose})}$ and ${}^2K_{d(\text{maltose})}$ are those [maltose] producing half Δk for saturable components 1 and 2. The results are: for k_{-1}, $k = 1.03 \pm 0.05$ s^{-1}, $\Delta k_1 = \Delta k_2 = 1.66 \pm 0.06$ s^{-1}, and ${}^1K_{d(\text{maltose})} = {}^2K_{d(\text{maltose})} = 53 \pm 7$ μM ($R^2 = 0.993$); for k_1, $k = 2.97 \pm 0.05$ $\mu M^{-1}\cdot s^{-1}$, $\Delta k_1 = -1.21 \pm 0.10$ $\mu M^{-1}\cdot s^{-1}$, $\Delta k_2 = -1.83 \pm 0.27$ $\mu M^{-1}\cdot s^{-1}$, ${}^1K_{d(\text{maltose})} = 0.52 \pm 0.14$ mM, and ${}^2K_{d(\text{maltose})} = 62.2 \pm 30.4$ mM ($R^2 = 0.998$). (B) $K_{d(app)}$ for CCB binding (μM, ordinate) is calculated as $k_{-1(app)}/k_{1(app)}$ (Figure 5A) and expressed as a function of [maltose] (mM, abscissa). The solid curve drawn through the points was computed by nonlinear regression assuming a fixed-site carrier according to eq 3 and has the following constants: $K_d = 0.37$ μM, $K_{M1} = 55.8$ mM, $K_{M2} = 0.057$ mM, $\beta = 0.93$, and $\alpha = 3.92$ ($R^2 = 0.993$). The dashed lines represent negative cooperative inhibition of CCB binding promoted by maltose binding to the import site (αK_{M2}) alone (- - -) or competitive inhibition of CCB binding produced by maltose binding at the export site (K_{M1}) alone (− −).

Accordingly, the data of Figures 3 and 4A have been analyzed assuming a fixed-site carrier mechanism. The curves drawn through the data were computed by nonlinear regression assuming a fixed-site carrier (see Materials and Methods and eqs 5 and 6 of the Discussion). This allows determination of k_1, k_{-1}, K_{M1} [the dissociation constant for intracellular maltose (M1) binding to the export site], K_{M2} [the dissociation constant for extracellular maltose (M2) binding to the export site], k_1' (the second-order rate constant for CCB binding to the M2·GLUT1 complex), k_{-1}' (the first-order rate constant for CCB dissociation from the M2·GLUT1·CCB complex), and β (a cooperativity factor describing how extracellular maltose binding to GLUT1 affects intracellular maltose binding to the export site). According to this analysis, rate constants describing CCB interaction with M2·GLUT1 (k_1' and k_{-1}') are 2−3-fold greater than the corresponding parameters for interaction with GLUT1 (k_1 and k_{-1}), and intracellular maltose binding to M2·GLUT1 occurs with greater affinity than intracellular maltose binding to GLUT1 ($\beta < 1$). Table 1 summarizes the results of several similar experiments made using maltose and purified GLUT1.

Unlike maltose, the *e2*-reactive ligand phloretin acts only to increase k_{obs} for CCB binding (Figure 6). The transported (*e1*- and *e2*-reactive and translocation-competent) sugars D-glucose and 3-*O*-methylglucose and the nontransported but *e1*- and *e2*-reactive sugars α-methylglucose, 4,6-*O*-ethylideneglucose, and maltotriose mimic the actions of maltose on k_{obs} for CCB binding (Table 1).

DISCUSSION

The glucose transporter of human erythrocytes is comprised of four copies of the membrane-spanning protein GLUT1 *(17)*. Each GLUT1 protein undergoes a reversible conformational change between two states. The *e1* state presents a sugar export pathway, and the *e2* state presents a sugar import pathway *(20, 21)*. This reversible conformational change is instrumental in effecting translocation of bound sugar across the membrane *(3)*. We have proposed that cooperative interactions between GLUT1 proteins give rise to more complex transport behavior *(22)*. Specifically, when one GLUT1 protein of the transporter complex presents an *e1* state, the adjacent subunit must present an *e2* state. In this way, each transporter (GLUT1 tetramer) can present two *e2* and two *e1* states simultaneously. The most important observation resulting from the present study is the demonstration that maltose (*e2*) and cytochalasin B (*e1*) binding states coexist in the purified glucose transporter. This allows critical evaluation of several hypotheses for GLUT1-mediated sugar transport.

The methods used in the present study differ from measurements of equilibrium CCB binding to the glucose transport protein *(7)*. The stopped-flow experiments reported here measure rate constants for CCB association with and CCB dissociation from GLUT1 present in unsealed proteoliposomes. CCB binds only to GLUT1 export *(e1)* sites; thus, the topology of CCB binding is unambiguous. Maltose, on the other hand, is a GLUT1 ligand that interacts with GLUT1 sugar import (*e2*) and sugar export (*e1*) sites. Because GLUT1 proteoliposomes are unsealed, maltose has unrestricted access to exofacial and endofacial domains of each GLUT1 molecule and can interact with both *e1* and *e2* sites if presented by the transporter.

The time-course of CCB-promoted GLUT1 fluorescence quenching is consistent with a second-order process limited by CCB interaction with the transport protein. It is important to ask, therefore, whether CCB access to the interior of GLUT1 proteoliposomes is limiting for GLUT1 fluorescence quenching (GLUT1 and thus *e1* sites are randomly oriented in the plasma membrane). Two lines of evidence argue

Table 1

sugar[b]	fixed-site carrier parameter[a]										
	k_{-1}[c]	k_1[d]	k_{-1}'[c]	k_1'[d]	K_d[e]	K_d'[e]	α[f]	β[f]	K_{M1}[g]	K_{M2}[g]	n[h]
none	1.0	2.9			0.4						
D-glucose	2.3	2.6	3.8	3.4	0.9	1.1	1.3	0.6	32.3	0.1	8
maltose	0.9	3.6	2.9	6.1	0.3	0.5	2.0	0.5	32.1	0.1	5
maltotriose	1.9	2.6	7.2	5.1	0.7	1.4	1.9	0.6	30.3	0.1	3
3OMG	2.0	3.0	6.0	5.1	0.7	1.2	1.8	0.4	26.3	1.0	2
ethylidene glucose	1.9	2.9	2.6	4.0	0.7	0.7	1.0	1.4	5.9	0.3	3
phloretin	1.5	2.6	165.9	4.5	0.6	37.3	64.6			0.3	3
mean[i]	1.7 ± 0.2	2.9 ± 0.1			0.57 ± 0.1						

[a] Parameters are described in Figure 7a and were computed by linear regression analysis of CCB modulation of k_{obs} (Figure 2A) or by nonlinear regression analysis of sugar modulation of k_{obs} for CCB binding to GLUT1 as in Figure 3. [b] CCB binding was determined in the absence (none) or presence of the sugars listed. [c] k_{-1} and k_{-1}' have units of s^{-1}. [d] k_1 and k_1' have units of $\mu M^{-1}\cdot s^{-1}$. [e] K_d and K_d' have units of μM and are calculated as k_{-1}/k_1 and k_{-1}'/k_1', respectively. [f] α and β are dimensionless cooperativity factors. [g] K_{M1} and K_{M2} have units of mM. [h] The number of times each experiment was performed in quadruplicate or more. [i] The average $\pm$ SEM of all experiments.

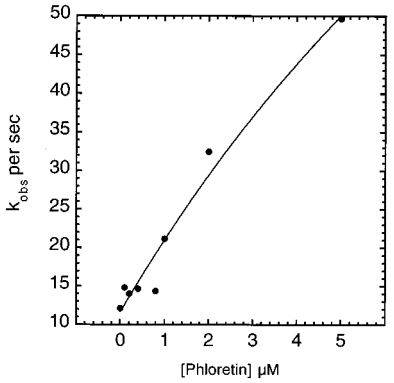

FIGURE 6: Effect of phloretin on k_{obs} for CCB (4 μM)-promoted GLUT1 fluorescence decay. GLUT1 and CCB solutions contained identical [phloretin] (0−10 μM) prior to rapid mixing. The experiment of Figure 1 was repeated at least 4 times at each phloretin concentration. Time-course data were averaged for each [phloretin] employed and analyzed as in Figure 1 to obtain k_{obs} for fluorescence decay. On the ordinate is k_{obs} in s^{-1}. On the abscissa is [phloretin] in μM. The curve drawn through the points was computed by nonlinear regression assuming that CCB and phloretin binding to GLUT1 is consistent with a fixed-site carrier mechanism (see Materials and Methods). According to this analysis, $k_{-1} = 1.47$ s^{-1}, $k_{-1}' = 165.9$ s^{-1}, $K_{M2} = 0.27$ μM, binding at the export site is undetectable, $k_1 = 2.55$ $\mu M^{-1}\cdot s^{-1}$, and $k_1' = 4.45$ $\mu M^{-1}\cdot s^{-1}$ ($R^2 = 0.97$). This experiment was repeated 2 additional times with similar results (see Table 1).

against the hypothesis that the present measurements are diffusion-limited. (1) The time-course of CCB-induced fluorescence quenching is consistent with a single exponential process. If CCB access to 50% of the *e1* sites was limited by diffusion, one would expect either biphasic quenching kinetics or an instantaneous quench (resulting from CCB interaction with GLUT1 *e1* sites at the outside of proteoliposomes) followed by a slower quench (resulting from CCB diffusion to and interaction with *e1* sites available at the interior of proteoliposomes). Neither result was observed. (2) The distance (λ_{avg}) that a sugar of average diffusion coefficient ($D = 1 \times 10^{-5}$ $cm^2\cdot s^{-1}$) *(23)* travels in 1.5 ms (the dead time of the instrument, t_d) is estimated as

$$\lambda_{avg} = \sqrt{2Dt_d} = 1.5\ \mu m$$

This distance is 6-fold greater than the upper diameter of unsealed GLUT1 proteoliposomes. These considerations argue strongly against a diffusion-limited process.

The basis of ligand-induced GLUT1 intrinsic tryptophan fluorescence quenching is not fully understood but may involve relocation of GLUT1 tryptophan 388 or 412 from an aqueous to a hydrophobic environment *(24−26)*. In the present study, we were unable to detect alterations in GLUT1 intrinsic fluorescence upon addition of GLUT1-reactive mono- or disaccharides whereas CCB binding promoted GLUT1 fluorescence quenching of about 5−10%. Previous equilibrium fluorescence measurements have reported that GLUT1-reactive mono- and disaccharides also promote quenching of GLUT1 intrinsic fluorescence although to a lesser degree than does CCB *(26−28)*. CCB is known to differ from maltose and D-glucose in its effects on Stern−Volmer plots of GLUT1 fluorescence quenching by KI or acrylamide *(24)*. Circular dichroism studies indicate that D-glucose binding to GLUT1 promotes increased GLUT1 ordered secondary structure *(29)*. CCB, while acting to inhibit D-glucose modulation of GLUT1, does not alter GLUT1 secondary structure *(29)*. These findings suggest that sugars and CCB interact with GLUT1 through distinct mechanisms. This behavior, in conjunction with differences in cell optics and wavelengths of emission sampling, may account for the apparent lack of effect of sugars on GLUT1 fluorescence in the present study. Studies of GalP (a bacterial homologue of GLUT1) also show that CCB but not substrate (galactose) promotes GalP intrinsic fluorescence quenching *(30)*.

CCB binding to GLUT1 may be reduced to a simple reaction of the type:

$$\text{GLUT1} + \text{CCB} \underset{k_{-1}}{\overset{k_1}{\rightleftharpoons}} \text{GLUT1}\cdot\text{CCB}$$

where k_1 and k_{-1} are second- and first-order rate constants for CCB interaction with GLUT1. At 20 °C, k_1 and k_{-1} are 2.8×10^6 $M^{-1}\cdot s^{-1}$ and 0.7 s^{-1}, respectively. The ratio k_{-1}/k_1 [0.25 μM CCB; $K_{d(app)}$ for CCB binding to GLUT1] is in close agreement with $K_{0.5}$ for CCB-induced equilibrium fluorescence quenching (0.24 μM CCB) and with $K_{d(app)}$ for [^{3}H]-CCB binding to GLUT1 (0.2 μM). This result confirms that CCB-promoted GLUT1 fluorescence quenching reflects a second-order process and forms a basis for additional experiments that can distinguish various carrier models for GLUT1-mediated sugar transport.

The simple carrier hypothesis (see Figure 7b) proposes that the glucose transporter alternately presents sugar import and sugar export sites to available substrate *(2, 3)*. The fixed-

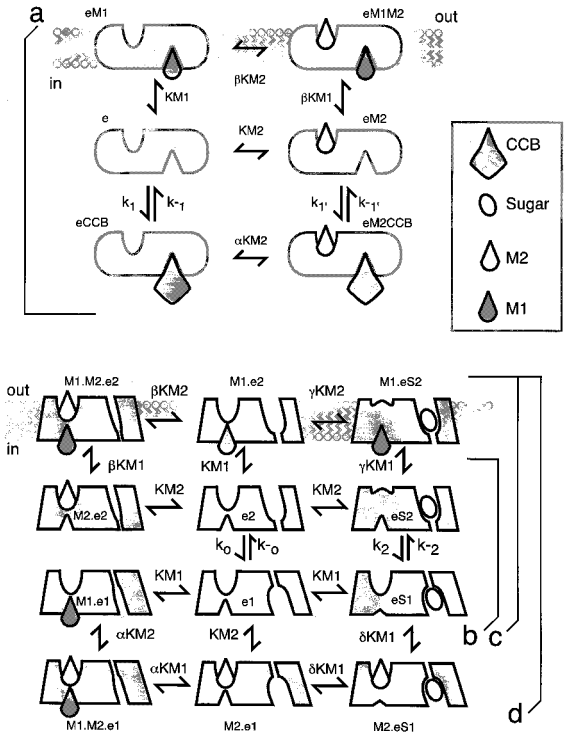

FIGURE 7: Models for GLUT1-mediated sugar transport shown in schematic King−Altman form. Each carrier state represents a hypothetical section (normal to the plane of the membrane bilayer) through the carrier. The upper and lower surfaces of each carrier state represent extra- (out) and intracellular (in) domains, respectively. (a) The fixed-site carrier (*e*) presents import and export sites simultaneously and may thus bind CCB and extracellular maltose (M2) simultaneously. Intracellular maltose (M1) and CCB compete directly for binding to the export site. Dissociation constants for M1 binding (K_{M1} and βK_{M1}) and M2 binding (K_{M2}, βK_{M2}, and αK_{M2}) are indicated. First- (k_{-1} and k_{-1}') and second-order (k_1 and k_1') rate constants for CCB interaction with the export site are indicated. (b) The simple carrier presents import (*e2*) and export (*e1*) sites sequentially. Catalytic domains of the simple carrier are indicated to the right of each carrier state as depressions and are superimposed on the shaded arrows drawn below each carrier isoform. Noncatalytic, inhibitor binding domains are indicated by unshaded depressions on the left half of each carrier state. When *e2* is presented but unoccupied, an extracellular inhibitor binding site (*i2*) is available. *i2* cannot exist when the carrier presents *e1*. Occupation of *i2* by extracellular maltose (M2) prevents *e2* occupation by extracellular transportable sugar (S2) and vice versa. When *e1* is presented but unoccupied, an intracellular inhibitor binding site (*i1*) is available. *i1* cannot exist when the carrier presents *e2*. *i2* cannot exist when the carrier presents *e1*. Thus, *i1* and *i2* are mutually exclusive for the simple carrier. Occupation of *i1* by intracellular maltose (M1) or CCB prevents *e1* occupation by intracellular transportable sugar (S1) and vice versa. *e2* and *e1* interconvert in the absence of S1 and S2 via relaxation steps k_o and k_{-o}. S1 and S2 are translocated via steps k_2 and k_{-2}. M2·*e2* and M1·*e1* are dead-end complexes. (c) The simple carrier with partial fixed-site inhibition. This form of the simple carrier can present *e2* and *i1* simultaneously but does not present *e1* and *i2* simultaneously. Thus, the carrier can be occupied simultaneously by S2 and CCB and by M2 and CCB but not by S2 and S1. (d) The simple carrier with fixed-site inhibition. The catalytic center of this carrier is the simple carrier, which undergoes *e1* − *e2* interconversion. The carrier also contains intracellular (*i1*) and extracellular (*i2*) inhibitor binding sites. *i1* and *e1* are mutually exclusive as are *i2* and *e2* and *e1* and *e2*. However, *i1* and *i2* can coexist as may *i1* and *e2* and *i2* and *e1*.

site carrier (Figure 7a) proposes that the transporter presents sugar import and sugar export pathways simultaneously *(1, 4, 5)*.

Maltose (a nontransportable but *e1*- and *e2*-reactive disaccharide) interactions with the simple carrier should be of the form:

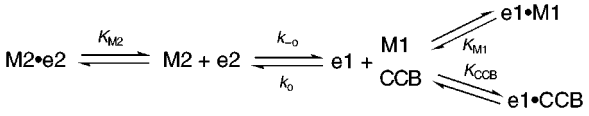

where K_{M1} and K_{M2} are dissociation constants for intra- and extracellular maltose (M1 and M2, respectively) binding to *e1* and *e2*, respectively. K_{CCB} is k_{-1}/k_1 (see above), and k_o and k_{-o} are first-order rate constants describing GLUT1 interconversions between *e1* and *e2* states in the absence of transportable sugars. Maltose is expected to competitively inhibit CCB binding by reducing available *e1* for interaction with CCB. According to this mechanism, K_{CCB} is given by

$$K_{CCB} = \frac{k_{-1}}{k_{1(app)}} \text{ where } k_{1(app)} = \frac{k_1}{1 + \frac{M1}{K_{M1}} + \frac{k_o}{k_{-o}}\left(1 + \frac{M2}{K_{M2}}\right)} \quad (1)$$

Thus, K_{CCB} increases linearly with increasing [maltose]. k_{obs} (the pseudo-first-order rate constant) for CCB binding is

$$k_{-1} + [CCB]\frac{k_1}{1 + \frac{M1}{K_{M1}} + \frac{k_o}{k_{-o}}\left(1 + \frac{M2}{K_{M2}}\right)} \quad (2)$$

Thus, k_{-1} is unchanged by maltose, but $k_{1(app)}$ falls with increasing concentrations of maltose.

The fixed-site carrier, *e*, can exist in any of six possible states in the presence of maltose and CCB (*e*, *e*·M1, *e*·M2, *e*·M1·M2, *e*·CCB, and *e*·CCB·M2). K_{CCB} for CCB binding to *e* is given by *(7, 8)*

$$K_{d(app)} = K_d\left\{\frac{1 + \frac{M1}{K_{M1}} + \frac{M2}{K_{M2}} + \frac{M1M2}{\beta K_{M1}K_{M2}}}{1 + \frac{M2}{\alpha K_{M2}}}\right\} \quad (3)$$

where $K_d = k_{-1}/k_1$ and α and β are dimensionless cooperativity factors describing how extracellular maltose binding to *e* affects the dissociation constants for CCB or intracellular maltose binding, respectively. Thus, $K_{d(app)}$ is affected by M2 only when $\alpha < 1$ or $\alpha > 1$ (CCB and M2 show cooperative binding). $K_{d(app)}$ increases linearly with M1.

If k_1 and k_{-1} for CCB interaction with *e* differ from those for CCB interaction with *e*·M2 (k_1' and k_{-1}'):

$$\alpha = \frac{k_{-1}'}{k_1'}\frac{k_1}{k_{-1}} \quad (4)$$

$$k_{-1(app)} = \frac{k_{-1} + k_{-1}'\frac{M2}{\alpha K_{M2}}}{1 + \frac{M2}{\alpha K_{M2}}} \quad (5)$$

Table 2

carrier mechanism[b]	V_{max}[a] zero-trans entry[c]	V_{max}[a] equilibrium exchange[d]
simple carrier (7b)	$\frac{[GLUT1]k_{-2}k_o}{k_o + k_{-2}\left\{1 + \frac{M1}{K_{M1}}\right\}}$	$\frac{[GLUT1]k_2k_{-2}}{k_2 + k_{-2}}$
simple carrier with partial fixed-site inhibition (7c)	$\frac{[GLUT1]k_ok_{-2}}{k_o\left\{1 + \frac{M1}{\gamma K_{M1}}\right\} + k_{-2}\left\{\frac{1 + M1}{K_{M1}}\right\}}$	$\frac{[GLUT1]k_2k_{-2}}{k_2\left\{1 + \frac{M1}{\gamma K_{M1}}\right\} + k_{-2}}$
simple carrier with fixed-site inhibition (7d)	$\frac{[GLUT1]k_ok_{-2}}{k_o\left\{1 + \frac{M1}{\gamma K_{2M1}}\right\} + k_{-2}\left\{1 + \frac{M1}{K_{M1}} + \frac{M2}{K_{1M2}} + \frac{M1M2}{\beta K_{M1}K_{1M2}}\right\}}$	$\frac{[GLUT1]k_2k_{-2}}{k_2\left\{1 + \frac{M1}{\gamma K_{2M1}}\right\} + k_{-2}\left\{1 + \frac{M2}{\delta K_{1M2}}\right\}}$
fixed-site carrier (7a)[e]	$\frac{[GLUT1]k_{-2}}{1 + \frac{CCB}{\alpha K_{CCB}} + \frac{M1}{\pi K_{M1}}}$	$\frac{[GLUT1](k_3 + k_{-3})}{2}$

[a] V_{max} is the maximum rate of transport achieved at saturating sugar concentrations. The steady-state solutions for V_{max} were obtained as in ref *8* and are expressed in terms of the constants shown in Figure 7 for each carrier mechanism. *S*1 and *S*2 are intra- and extracellular concentrations of transportable sugar, respectively. *M*1 and *M*2 are intra- and extracellular concentrations of nontransportable, transport inhibitors (e.g., maltose), respectively. *CCB* is the cytochalasin B concentration and is interchangeable with M1. [b] The carrier mechanisms are those depicted schematically in Figure 7a−d. [c] Steady-state sugar uptake in the absence of intracellular sugar. [d] Unidirectional sugar uptake or exit when intracellular [sugar] = extracellular [sugar]. [e] k_{-2} is the rate of translocation of sugar through the $e{\cdot}S_2$ complex. k_3 and k_{-3} are rate constants for translocation of S_1 and S_2 through the $eS_1{\cdot}S_2$ complex, respectively. α and π are $k_1k_{-1}/k_{-1}k_1'$ when the ligand pairs are S_2 and CCB and S_2 and M1, respectively.

$$k_{1(app)} = \frac{k_1 + k_1'\frac{M2}{\alpha K_{M2}}}{1 + \frac{M1}{K_{M1}} + \frac{M2}{K_{M2}} + \frac{M1M2}{\beta K_{M1}K_{M2}}} \qquad (6)$$

Thus, if $k_{-1} \neq k_{-1}'$, $k_{-1(app)}$ increases ($k_{-1} < k_{-1}'$) or decreases ($k_{-1} > k_{-1}'$) in a saturable manner with M2 with $K_{0.5}$ for $M2 = \alpha K_{M2}$ (see eq 5). In the absence and presence of M2, $k_{1(app)}$ decreases in a saturable manner with M1 (eq 6).

Our results show that k_{obs} for CCB binding increases at low [maltose] and falls at higher [maltose]. Analysis of the [CCB] dependence of this phenomenon indicates that $k_{-1(app)}$ increases in a saturable manner with low [maltose] whereas $k_{1(app)}$ decreases in a biphasic manner ($K_{M2} \neq K_{M1}$) with increasing [maltose]. This result is inconsistent with predictions of the simple carrier hypothesis (k_{-1} is unchanged by maltose) and supports rejection of this model as an adequate description of ligand binding to the sugar transporter of erythrocytes.

This conclusion (maltose and CCB binding are not mediated by a simple carrier) assumes that CCB and maltose interact with GLUT1 catalytic sites. It is possible, however, that the transport pathway of GLUT1 indeed functions as a simple carrier but that the inhibitor binding domains are unrelated to and, thus, independent of catalytic sites.

We therefore considered ligand binding to two variations of simple carrier. The simple carrier with fixed-site inhibition (Figure 7, mechanism d) describes a simple carrier mechanism in which inhibitor and sugar binding sites are distinct. Thus, the intracellular binding site for M1 does not correspond to *e1* (the S1 binding site). Nevertheless, the carrier cannot bind S1 and M1 (M1 represents intracellular maltose or CCB) simultaneously because these sites are mutually exclusive. Similarly, the extracellular binding site for M2 does not correspond to *e2* (the S2 binding site), yet the carrier cannot bind S2 and M2 simultaneously. This mechanism does allow for simultaneous occupancy of GLUT1 by trans ligands (e.g., M1 and M2, M1 and S2, S1 and M2 but not by S1 and S2).

The simple carrier with partial fixed-site inhibition (Figure 7, mechanism c) is a variant of the simple carrier mechanism with fixed-site inhibition. This mechanism allows for simultaneous occupancy of GLUT1 by only some trans ligands (e.g., M1 and M2, M1 and S2, but not by S1 and S2 or by S1 and M2).

We examined the predicted effects (see Table 2) of M1 and M2 on zero-trans and equilibrium exchange sugar entry mediated by either of these theoretical mechanisms. This is particularly useful because the effects of M1 and M2 on human erythrocyte zero-trans and equilibrium exchange sugar fluxes are well characterized *(4, 8)*. Zero-trans entry describes sugar uptake into sugar-free cells. Equilibrium exchange transport describes unidirectional sugar uptake or efflux when the concentration of sugar on either side of the membrane is identical. M1 is known to be a noncompetitive inhibitor while M2 is a competitive inhibitor of zero-trans sugar uptake in human red cells *(8)*. M1 and M2 are competitive inhibitors of human erythrocyte equilibrium exchange sugar transport *(4, 8)*.

Solutions for steady-state zero-trans and equilibrium exchange transport mediated by the simple carrier with fixed-site inhibition show that M2 acts as a noncompetitive inhibitor of zero-trans entry and M1 and M2 serve as noncompetitive inhibitors of equilibrium exchange (Table 1). For the simple carrier with partial fixed-site inhibition, M1 serves as a noncompetitive inhibitor of equilibrium exchange. These predictions run counter to experimental

findings. We therefore conclude that simple carriers with fixed or partial fixed-site inhibition cannot account for CCB and maltose binding to and inhibition of the glucose transporter of erythrocytes.

At this time, no variation of the simple carrier mechanism accounts adequately for sugar modulation of CCB binding to the human erythrocyte sugar transporter (see here and ref *9*) or for sugar modulation of CCB inhibition of erythrocyte sugar transport *(8*). We conclude that the continued use of this hypothetical transport mechanism to describe human erythrocyte GLUT1-mediated sugar transport and ligand binding is no longer justified.

The fixed-site carrier, however, continues to present a useful framework for interpretation of human erythrocyte sugar transport and sugar transporter ligand binding. Nonlinear regression analysis of maltose modulation of k_{obs} for CCB binding to GLUT1 within the context of the fixed-site carrier mechanism permits computation of all parameters for fixed-site carrier interaction with CCB, M1, and M2 (see Table 1 and Figures 3 and 4). These parameters have also been computed for modulations of CCB binding by maltotriose, ethylidene glucose, glucose, 3-*O*-methylglucose, and phloretin (Table 1). Our results show (assuming sugar transport is mediated by a fixed carrier) that maltose binding to the *e2* site occurs with relatively high affinity ($K_{M2} = 1.5$ mM). Maltose occupancy of *e2* doubles the on-rate constant (k_1') for CCB binding at *e1* and increases the off-rate constant (k_{-1}') for CCB binding at *e1* by 4-fold. The net effect is a doubling of $K_{d(app)}$ for CCB binding to *e1*. Similarly, CCB binding to *e1* increases $K_{d(app)}$ for M2 binding to *e2* by the same extent. Thus, *e1* and *e2* sites within a single transport unit interact with negative cooperativity when the ligand binding pair is CCB and extracellular maltose. This result is consistent with previous equilibrium CCB binding studies from this laboratory *(7, 8*) in which $K_{d(app)}$ and $K_{i(app)}$ for CCB and maltose binding to or inhibition of the sugar transporter were determined. Our findings also suggest that *e1* and *e2* sites interact with positive cooperativity when the ligand binding pair is extracellular and intracellular maltose.

Previous equilibrium CCB binding studies from this laboratory *(7, 8*) have suggested that extracellular D-glucose is without net effect on $K_{d(app)}$ for CCB binding to *e1*. Our present study confirms this but expands this observation by demonstrating that *e2* occupancy by D-glucose increases both k_1 and k_{-1} proportionally for CCB binding to and dissociation from *e1*. This is not a signature property of transportable sugars, however. Transport-competent 3-*O*-methylglucose resembles maltose in its ability to increase k_{-1} to a greater extent than its effect on k_1.

Consistent with our previous studies *(7, 8*), phloretin interaction with *e2* results in an extreme increase in $K_{d(app)}$ for CCB binding to *e1*. The present study permits us to conclude that this results almost exclusively from decreased stability of the phloretin·*e2*·*e1*·CCB complex (k_{-1} for CCB dissociation is increased 110-fold whereas k_1 for CCB binding is doubled). The net effect is that $K_{d(app)}$ for CCB binding increases by some 60-fold (compare with 45-fold in ref *7*).

One unexpected finding was obtained. Ethylidene glucose failed to promote negative cooperativity between extracellular and CCB binding sites ($k_{-1}/k_1 = k_{-1}'/k_1'$). Previous equilibrium [^{3}H]-CCB binding studies support the conclusion that extracellular ethylidene glucose promotes a GLUT1 state in which $k_{-1}/k_1 < k_{-1}'/k_1'$ *(7*). It is possible that strong UV absorption by ethylidene glucose compromises the accuracy of the present measurements.

CONCLUSION

The purified, nonreduced glucose transporter of human erythrocytes and the erythrocyte membrane-resident glucose transporter bind sugars and cytochalasin B simultaneously. Occupation of transporter sugar binding site(s) by a variety of sugars modulates cytochalasin B binding to and dissociation from the cytochalasin B binding pocket. If cytochalasin B and high-affinity sugar binding sites correspond to sugar export and sugar import sites, respectively, the sugar transport does not function as a simple carrier. Rather, the transporter must present sugar import and export sites simultaneously.

REFERENCES

1. Naftalin, R. J., and Holman, G. D. (1977) in *Membrane transport in red cells* (Ellory, J. C., and Lew, V. L., Eds.) pp 257−300, Academic Press, New York.
2. Lieb, W. R., and Stein, W. D. (1974) *Biochim. Biophys. Acta 373*, 178−196.
3. Widdas, W. F. (1952) *J. Physiol. (London) 118*, 23−39.
4. Basketter, D. A., and Widdas, W. F. (1978) *J. Physiol. (London) 278*, 389−401.
5. Carruthers, A. (1991) *Biochemistry 30*, 3898−3906.
6. Krupka, R. M., and Devés, R. (1981) *J. Biol. Chem. 256*, 5410−5416.
7. Helgerson, A. L., and Carruthers, A. (1987) *J. Biol. Chem. 262*, 5464−5475.
8. Carruthers, A., and Helgerson, A. L. (1991) *Biochemistry 30*, 3907−3915.
9. Cloherty, E. K., Heard, K. S., and Carruthers, A. (1996) *Biochemistry 35*, 10411−10421.
10. Segel, I. H. (1975) in *Enzyme Kinetics*, pp 100−125, Wiley, New York.
11. Zottola, R. J., Cloherty, E. K., Coderre, P. E., Hansen, A., Hebert, D. N., and Carruthers, A. (1995) *Biochemistry 34*, 9734−9747.
12. Cairns, M. T., Alvarez, J., Panico, M., Gibbs, A. F., Morris, H. R., Chapman, D., and Baldwin, S. A. (1987) *Biochim. Biophys. Acta 905*, 295−310.
13. Jung, C. Y., and Rampal, A. L. (1977) *J. Biol. Chem. 252*, 5456−5463.
14. Peterman, B. F. (1979) *Anal. Biochem. 93*, 442−444.
15. LeFevre, P. G. (1961) *Pharmacol. Rev. 13, 39−70.*
16. Carruthers, A., and Melchior, D. L. (1984) *Biochemistry 23*, 6901−6911.
17. Hebert, D. N., and Carruthers, A. (1992) *J. Biol. Chem. 267*, 23829−23838.
18. Coderre, P. E., Cloherty, E. K., Zottola, R. J., and Carruthers, A. (1995) *Biochemistry 34*, 9762−9773.
19. Fierke, C. A., and Hammes, G. A. (1996) in *Contemporary Enzyme Kinetics and Mechanism* (Purich, D. L., Ed.) pp 1−35, Academic Press, San Diego.
20. Sogin, D. C., and Hinkle, P. C. (1980) *Biochemistry 19*, 5417−5420.
21. Baldwin, S. A., Baldwin, J. M., and Lienhard, G. E. (1982) *Biochemistry 21*, 3836−3842.
22. Zottola, R. J., Cloherty, E. K., Coderre, P. E., Hansen, A., Hebert, D. N., and Carruthers, A. (1995) *Biochemistry 34*, 9734−9747.
23. Baker, P. F., and Carruthers, A. (1981) *J. Physiol. (London) 316*, 481−502.
24. Pawagi, A. B., and Deber, C. M. (1990) *Biochemistry 29*, 950−955.

25. Garcia, J. C., Strube, M., Leingang, K., Keller, K., and Mueckler, M. M. (1992) *J. Biol. Chem. 267*, 7770−7776.
26. Chin, J. J., Jhun, B. H., and Jung, C. Y. (1992) *Biochemistry 31*, 1945−1951.
27. Carruthers, A. (1986) *Biochemistry 25*, 3592−3602.
28. Gorga, F. R., and Lienhard, G. E. (1982) *Biochemistry 21*, 1905−1908.
29. Pawagi, A. B., and Deber, C. M. (1987) *Biochem. Biophys. Res. Commun. 145*, 1087−1091.
30. Walmsley, A. R., Martin, G. E., and Henderson, P. J. (1994) *J. Biol. Chem. 269*, 17009−17019.

BI990130O